Influence of polarity on carrier transport in semipolar (20$\bar{2}$1) and (20$\bar{2}\bar{1}$) multiple-quantum-well light-emitting diodes

Yoshinobu Kawaguchi,[1,2,a)] Chia-Yen Huang,[1,b)] Yuh-Renn Wu,[3] Qimin Yan,[1]
Chih-Chien Pan,[1] Yuji Zhao,[4] Shinichi Tanaka,[1] Kenji Fujito,[5] Daniel Feezell,[1]
Chris G. Van de Walle,[1] Steven P. DenBaars,[1,4] and Shuji Nakamura[1,4]

[1]*Department of Materials, University of California, Santa Barbara, California 93106, USA*
[2]*Advanced Technology Research Laboratories, Sharp Corporation, 2613-1 Ichinomoto-cho, Tenri, Nara 632-8567, Japan*
[3]*Institute of Photonics and Optoelectronics and Department of Electrical Engineering, National Taiwan University, Taipei 10617, Taiwan*
[4]*Department of Electrical and Computer Engineering, University of California, Santa Barbara, California 93106, USA*
[5]*Optoelectronics Laboratory, Mitsubishi Chemical Corporation, 1000 Higashi-mamiana, Ushiku, Ibaraki 300-1295, Japan*

We investigate the influence of polarity on carrier transport in single-quantum-well and multiple-quantum-well (MQW) light-emitting diodes (LEDs) grown on the semipolar (20$\bar{2}$1) and (20$\bar{2}\bar{1}$) orientations of free-standing GaN. For semipolar MQW LEDs with the opposite polarity to conventional Ga-polar *c*-plane LEDs, the polarization-related electric field in the QWs results in an additional energy barrier for carriers to escape the QWs. We show that semipolar (20$\bar{2}\bar{1}$) MQW LEDs with the same polarity to Ga-polar *c*-plane LEDs have a more uniform carrier distribution and lower forward voltage than (20$\bar{2}$1) MQW LEDs. © *2012 American Institute of Physics*. [http://dx.doi.org/10.1063/1.4726106]

Multiple-quantum-well (MQW) structures are frequently used to improve the performance of GaN-based light-emitting devices such as light-emitting diodes (LEDs) and laser diodes (LDs). For LDs, MQW structures are used to enhance gain and optical confinement. For LEDs, MQW structures are used to reduce droop by increasing the active region volume and lowering the average carrier density. However, the achievable improvement is limited because of an uneven carrier distribution among the quantum wells (QWs) in conventional c-plane MQW LEDs (Refs. [1] and [2]). The large strain-induced polarization in the InGaN QWs is one of the major causes of the uneven carrier distribution.[3] The QW nearest to the p-side has been experimentally observed to dominate the light emission due to poor hole injection efficiency.[1,2,4–7] Different barrier designs such as barrier doping[8,9] and compositionally graded InGaN barriers[10,11] have been applied to improve the hole injection efficiency between the QWs. Recently, GaN-based light-emitting devices grown on semipolar planes have been extensively studied due to their reduced polarization-related electric fields.[12,13] High-performance LEDs and LDs in the green region have been achieved on several semipolar planes. For example, high-power green LEDs were demonstrated on the (11$\bar{2}$2) (Refs. [14] and [15]) and (20$\bar{2}$1) (Ref. [16]) planes and low-threshold green LDs were also shown on the (20$\bar{2}$1) plane.[17–19] Devices grown on the (20$\bar{2}\bar{1}$) plane have also attracted considerable attention with reports of low droop[20] and high wavelength stability.[21] Sizov *et al.* conducted a detailed investigation on the impact of polarization-related electric fields on the carrier transport for nonpolar

and semipolar planes with ballistic transport models.[22] The study indicated that nonpolar and semipolar MQW devices have improved carrier transport compared to conventional *c*-plane devices because of their eliminated or reduced polarization-related electric fields. However, the carrier transport properties among different semipolar planes have not been fully investigated. Since the magnitudes and directions of polarization-related electric fields are different among various semipolar planes, the carrier transport properties are also expected to be different. In this paper, MQW LEDs grown on semipolar (20$\bar{2}$1) and (20$\bar{2}\bar{1}$) planes were investigated. Due to the same in-plane crystal geometry, these two planes theoretically have equal magnitudes of polarization-related electric fields; however, the directions of the polarization-related electric fields are opposite due to their opposite polarity.

LEDs with different numbers of QWs (n = 1, 2, 3) were grown on both (20$\bar{2}$1) and (20$\bar{2}\bar{1}$) planes by metalorganic chemical vapor deposition (MOCVD) on free-standing GaN substrates manufactured by Mitsubishi Chemical Corporation. The epitaxial structures all consisted of a 1 μm Si-doped n-GaN layer, an unintentionally doped active region with an InGaN/GaN QW/barrier structure, a 15 nm Mg-doped p-AlGaN electron-blocking layer (EBL) and a 120 nm Mg-doped p-GaN layer. The thicknesses of the QWs and the barrier layers between QWs are estimated to be 3 nm and 20 nm, respectively. The emission wavelengths ranged from 475 nm to 485 nm for all LEDs and were controlled by tuning the growth temperature of the active region. Photoluminescence (PL) measurements were conducted by using a 405 nm violet LD as an excitation light source. Electroluminescence (EL) measurements were done under constant injection current density (I = 20 mA) with Pd/Au as the

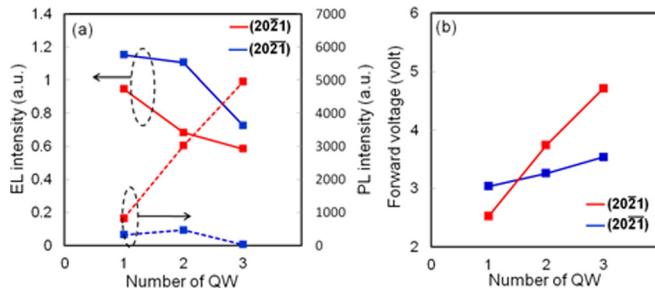a)kawaguchi.yoshinobu@sharp.co.jp.
b)chiayen@umail.ucsb.edu.

FIG. 1. (a) Relative EL and PL intensities and (b) forward voltages at 20 A/cm^2 for $(20\bar{2}1)$ and $(20\bar{2}\bar{1})$ LEDs with different numbers of quantum wells.

p-contact. The injection area was a circle with a radius of 40 μm.

Figure 1(a) shows the relative EL under DC 20 mA and PL intensities for all LEDs. The intensities decreased for higher numbers of QWs for both $(20\bar{2}1)$ and $(20\bar{2}\bar{1})$ LEDs. For $(20\bar{2}1)$ LEDs, the drop in EL intensities is more significant from n = 1 to n = 2. However, for $(20\bar{2}\bar{1})$ LEDs, the drop of intensity is more significant from n = 2 to n = 3. The drop in EL intensity with higher numbers of QWs can be attributed to deterioration of the QW crystal quality or to carrier transport issues between QWs. The PL intensities of $(20\bar{2}1)$ LEDs increased linearly with the number of QWs due to the increased active volume. Therefore, the drop of EL intensity is not attributed to the deterioration of the QW crystal quality. On the contrary, the PL intensity of the $(20\bar{2}\bar{1})$ LEDs only increases slightly from n = 1 to n = 2, but decreases significantly from n = 2 to n = 3, indicating possible deterioration of the crystal quality with increasing numbers of quantum wells. Figure 2 shows cathodoluminescence images for $(20\bar{2}\bar{1})$ LEDs with n = 2 and n = 3. The threading dislocation density is observed to increase when increasing from n = 2 to n = 3. Therefore, the drop in EL intensity of the LEDs in Figure 1(a) is likely explained by the addition of new threading dislocations that arise beyond a certain active region thickness for the case of n = 3. The forward voltages under 20 A/cm^2 injection current are shown in Figure 1(b). The forward voltages of $(20\bar{2}1)$ and $(20\bar{2}\bar{1})$ LEDs both increased monotonically. However, the increment of forward voltage with an additional QW is much more significant for $(20\bar{2}1)$ LEDs. These results present evidence that carrier transport issues may be more pronounced in $(20\bar{2}1)$ MQW LEDs compared to $(20\bar{2}\bar{1})$ MQW LEDs. In the following sections, dichromatic LEDs and band diagram simulations
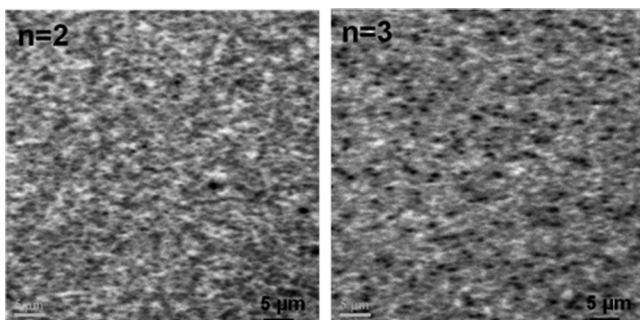
are utilized to compare the hole transport in $(20\bar{2}1)$ and $(20\bar{2}\bar{1})$ LEDs both experimentally and theoretically.

To examine the carrier transport phenomena in $(20\bar{2}1)$ and $(20\bar{2}\bar{1})$ LEDs, two sets of dichromatic LEDs were grown on both planes with two QWs emitting light in different wavelength region. The first set of LEDs (aquamarine-violet LEDs) have an aquamarine QW ($\lambda \sim 480$ nm, 28%–30% In) near the n-side and a violet QW near the p-side ($\lambda \sim 425$ nm, 14%−16% In), and the second set has a reversed order of QWs (violet-aquamarine LEDs). The wavelength was controlled by adjusting the growth temperature in the QWs. Because the band offsets and polarization-related electric fields in the violet QW are around half the magnitude of those in the aquamarine QW, the influence of the violet QW on carrier transport is expected to be minor. Therefore, the emission in the violet region is an indicator of electron injection efficiency for the aquamarine-violet LEDs and an indicator of the hole injection efficiency for the violet-aquamarine LEDs. For the aquamarine-violet LEDs, the EL spectrum under DC 20 mA injection is shown in Figure 3(a). Because of the large conduction band offset of the aquamarine QW, most of the electrons are confined in the aquamarine QW, resulting in a dominant emission in aquamarine region. The presence of the violet peak indicated that a certain portion of electrons were still injected into the QW at p-side. The EL spectra for the $(20\bar{2}1)$ and $(20\bar{2}\bar{1})$ LEDs were similar, which suggests the influence of polarity on electron transport is less significant. On the contrary, as shown in Figure 3(b), the EL spectra were quite different for the $(20\bar{2}1)$ and $(20\bar{2}\bar{1})$ violet-aquamarine LEDs. The diminished violet peak in the $(20\bar{2}1)$ LEDs indicates that most of the holes populate the QW near the p-side. Conversely, for the $(20\bar{2}\bar{1})$ LEDs, the comparable magnitudes of the violet and aquamarine peaks indicate a more effective hole transport across the aquamarine QW.

To confirm the influence of polarity on the hole transport, the number of aquamarine QWs was increased in the violet-aquamarine LEDs (n = 1, 2, 3), as schematically shown in Figure 4(a). The normalized EL spectra for $(20\bar{2}\bar{1})$ and $(20\bar{2}1)$ dichromatic MQW LEDs under 20 mA injection are shown in Figures 4(b) and 4(c), respectively. As n increases for the $(20\bar{2}\bar{1})$ LEDs, the emission intensity in the aquamarine region decreases due to the deterioration of crystal
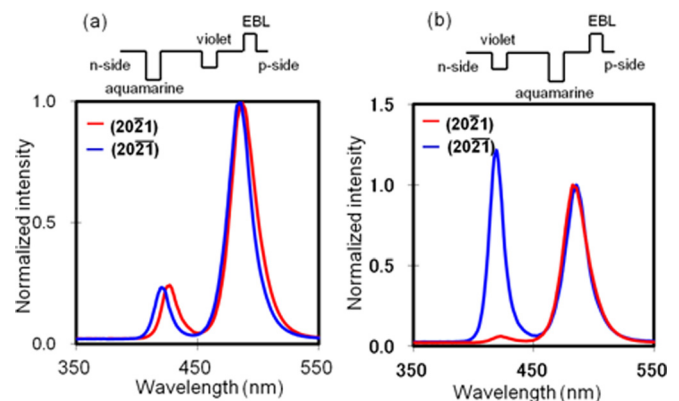

FIG. 2. Cathodoluminescence images of $(20\bar{2}\bar{1})$ LEDs with n = 2 (left) and n = 3 (right).

FIG. 3. EL spectra for dichromatic (a) aquamarine-violet and (b) violet-aquamarine $(20\bar{2}1)$ and $(20\bar{2}\bar{1})$ LEDs. The schematic structures are also illustrated above the spectra.
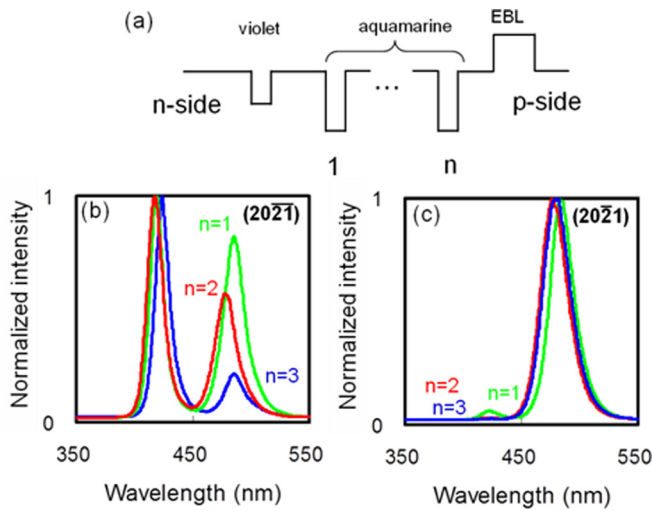
FIG. 4. (a) Schematic structures and EL spectra for (b) $(20\bar{2}\bar{1})$ and (c) $(20\bar{2}1)$ dichromatic LEDs with different numbers of aquamarine quantum wells.

quality as described in Figure 2, but holes still reach the violet QW near the n-side. For the $(20\bar{2}1)$ LEDs, no emission in the violet region is observed for n = 2 and n = 3. These results suggest that the drop in EL intensity and the increase in forward voltage for higher n in the $(20\bar{2}1)$ LEDs in Figure 1 are caused by poor hole injection and an uneven hole distribution, which is consistent with previous studies on $(20\bar{2}1)$ LEDs.[23]

Band diagram simulations were also conducted to investigate the origin of the different hole injection efficiencies for the $(20\bar{2}1)$ and $(20\bar{2}\bar{1})$ LEDs. Conventional drift-diffusion models have been effectively utilized to describe the carrier transport in c-plane violet and blue LEDs,[22,24,25] but the large magnitude of the polarization-related electric fields in c-plane green LEDs may preclude the use of these

models. However, since the magnitudes of the polarization-related electric fields in semipolar $(20\bar{2}1)$ and $(20\bar{2}\bar{1})$ green LEDs are similar to those in violet c-plane LEDs,[13] conventional drift-diffusion models can be utilized to examine the carrier transport for these semipolar green LEDs. A self-consistent 1D Poisson, drift-diffusion and Schrödinger numerical solver[26] was applied to calculate the band structure, carrier density, eigen-values, and wavefunctions. The calculated band diagrams for double-quantum-well (DQW) $(20\bar{2}1)$ and $(20\bar{2}\bar{1})$ LEDs under the same applied bias ($V_f = 3.1$ V) are shown in Figures 5(a) and 5(b), respectively. The epilayer structures and doping profiles of the LEDs in Figure 1 were utilized for all simulations. As seen in Figure 5, the barrier height for hole injection from the EBL to the topmost QW is lower for the $(20\bar{2}1)$ LED because the polarization-related field in the topmost barrier is antiparallel to the built-in electric field in the p-n junction, which is similar to the case of N-polar c-plane. As a result, the single-quantum-well (SQW) $(20\bar{2}1)$ LED has a lower forward voltage than the SQW $(20\bar{2}\bar{1})$ LED, as shown in Figure 1(b), and is consistent with the observed low turn-on voltages in N-polar SQW green LEDs.[27] However, for the $(20\bar{2}1)$ LEDs, the holes are decelerated by the reversed polarization-related electric field in the QW. Therefore, the injected holes are more likely to be captured in the QW or scattered at the hetero-interface in $(20\bar{2}1)$ LEDs. The energy differences between the hole ground-state and the quantum barrier are also illustrated in Figure 5(c). The barrier height for captured holes to escape the QW is significantly higher in $(20\bar{2}1)$ LEDs, and is attributed to the polarization-related electric fields in the QW. As a result, the calculated current density is lower for the $(20\bar{2}1)$ DQW LEDs. Theoretically, the polarization-related electric fields in the QW should also lead to a similar energy barrier for captured electrons to escape the QW in $(20\bar{2}1)$ LEDs. However, secondary ion
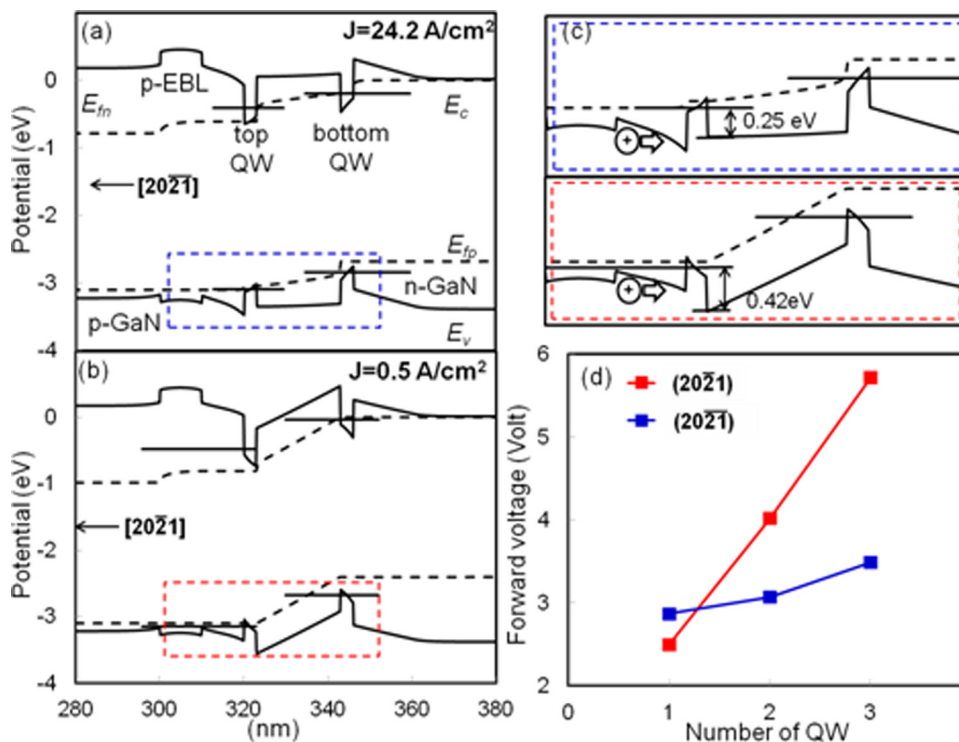

FIG. 5. Band diagrams for (a) $(20\bar{2}\bar{1})$ and (b) $(20\bar{2}1)$ double-quantum-well LEDs under 3.1 V forward bias. (c) Magnification of band diagrams at highlighted area. (d) Calculated forward biases under 20 A/cm² injection current for $(20\bar{2}1)$ and $(20\bar{2}\bar{1})$ LEDs with different number of QWs.
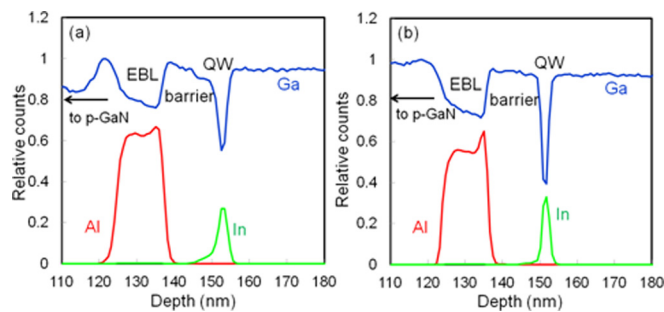
FIG. 6. Secondary ion mass spectroscopy measurement of (a) (20$\bar{2}$1) and (b) (20$\bar{2}\bar{1}$) LEDs.

mass spectroscopy measurements indicate that the interfaces between the QW and barriers are not particularly abrupt in the (20$\bar{2}$1) LEDs (Figure 6). The diffusive interface lowers the effective energy barrier for electron transport in (20$\bar{2}$1) LEDs, compensating the barrier generated by polarization-related electric fields in the QWs. Additionally, electrons also have a higher probability of experiencing ballistic injection without being captured by the QW because of their smaller effective mass and larger conduction band offset. Therefore, the influence of polarity on electron transport is expected to be less significant for these semipolar LEDs.

Figure 5(d) shows the calculated forward voltages under equal injection current density (20 A/cm^2) for (20$\bar{2}$1) and (20$\bar{2}\bar{1}$) LEDs with different numbers of QWs using the same structure as in Figure 1. The results show identical trends with the experimental data shown in Figure 1(b). The (20$\bar{2}$1) SQW LEDs have a lower forward voltage because the barrier height for carrier injection into the first QW is smaller. However, the polarization-related electric fields in the QWs of (20$\bar{2}$1) MQW LEDs hinder carrier transport between the QWs, resulting in higher forward voltages for (20$\bar{2}$1) MQW LEDs. The discrepancy between the calculated and experimental forward voltages for the (20$\bar{2}$1) LEDs is explained by the reduced energy barriers that result from the diffusive QW/barrier interfaces described above. For example, implementing a 5 nm graded InGaN barrier above the QWs with 5% In at the QW/barrier interfaces lowers the calculated forward voltage to 4.7 V in the n = 3 case, which is in good agreement with the experimental data of Figure 1(b).

In conclusion, we have investigated the influence of polarity on carrier transport in SQW and MQW LEDs grown on semipolar (20$\bar{2}$1) and (20$\bar{2}\bar{1}$) planes. With inverse polarization to Ga-polar LEDs, (20$\bar{2}$1) SQW LEDs showed lower forward voltages because of the reduced energy barrier height to the QW. However, the forward voltages increase rapidly for (20$\bar{2}$1) MQW LEDs. Due to the absence of additional energy barriers from polarization-related electric fields in the QW, the hole transport in semipolar (20$\bar{2}\bar{1}$) MQW LEDs is improved compared to that in semipolar (20$\bar{2}$1) MQW LEDs.

[1]A. David, M. J. Grundmann, J. F. Kaeding, N. F. Gardner, T. G. Mihopou-los, and M. R. Krames, Appl. Phys. Lett. **92**, 053502 (2008).
[2]J. P. Liu, J. H. Ryou, R. D. Dupuis, J. Han, G. D. Shen, and H. B. Wang, Appl. Phys. Lett. **93**, 021102 (2008).
[3]M. H. Kim, M. F. Schubert, Q. Dai, J. K. Kim, E. F. Schubert, J. Piprek, and Y. Park, Appl. Phys. Lett. **91**, 183507 (2007).
[4]Y. L. Li, T. Gessmann, E. F. Schubert, and J. K. Sheu, J. Appl. Phys. **94**, 2167 (2003).
[5]M. Peter, A. Laubsch, P. Stauss, A. Walter, J. Baur, and B. Hahn, Phys. Status Solidi C **5**, 2050 (2008).
[6]B. Galler, A. Laubsch, A. Wojcik, H. Lugauer, A. Gomez-Iglesias, M. Sabathil, and B. Hahn, Phys. Status Solidi C **8**, 2372 (2011).
[7]J. H. Zhu, S. M. Zhang, H. Wang, D. G. Zhao, J. J. Zhu, Z. S. Liu, D. S. Jiang, Y. X. Qiu, and H. Yang, J. Appl. Phys. **109**, 093117 (2011).
[8]J. Xie, X. Ni, Q. Fan, R. Shimada, Ü. Özgür, and H. Morkoç, Appl. Phys. Lett. **93**, 121107 (2008).
[9]S. H. Han, C. Y. Cho, S. J. Lee, T. Y. Park, T. H. Kim, S. H. Park, S. W. Kang, J. W. Kim, Y. C. Kim, and S. J. Park, Appl. Phys. Lett. **96**, 051113 (2010).
[10]C. H. Wang, S. P. Chang, P. H. Ku, J. C. Li, Y. P. Lan, C. C. Lin, H. C. Yang, H. C. Kuo, T. C. Lu, S. C. Wang, and C. Y. Chang, Appl. Phys. Lett. **99**, 171106 (2011).
[11]C. S. Xia, Z. M. Simon Li, W. Lu, Z. H. Zhang, Y. Sheng, and L. W. Cheng, Appl. Phys. Lett. **99**, 233501 (2011).
[12]T. Takeuchi, H. Amano, and I. Akasaki, Jpn. J. Appl. Phys. **39**, 413 (2000).
[13]A. E. Romanov, T. J. Baker, S. Nakamura, and J. S. Speck, J. Appl. Phys. **100**, 023522 (2006).
[14]M. Funato, M. Ueda, Y. Kawakami, Y. Narukawa, T. Kosugi, M. Takaha-shi, and T. Mukai, Jpn. J. Appl. Phys, **45**, L659 (2006)
[15]H. Sato, A. Tyagi, H. Zhong, N. Fellows, R. B. Chung, M. Saito, K. Fujito, J. S. Speck, S. P. DenBaars, and S. Nakamura, Phys. Status Solidi (RRL) **1**, 162 (2007).
[16]S. Yamamoto, Y. Zhao, C. C. Pan, R. B. Chung, K. Fujito, J. Sonoda, S. P. DenBaars, and S. Nakamura, Appl. Phys. Express **3**, 122102 (2010).
[17]Y. Enya, Y. Yoshizumi, T. Kyono, K. Akita, M. Ueno, M. Adachi, T. Sumitomo, S. Tokuyama, T. Ikegami, K. Katayama, and T. Nakamura, Appl. Phys. Express **2**, 082101 (2009).
[18]Y. Yoshizumi, M. Adachi, Y. Enya, T. Kyono, S. Tokuyama, T. Sumi-tomo, K. Akita, T. Ikegami, M. Ueno, K. Katayama, and T. Nakamura, Appl. Phys. Express **2**, 092101 (2009).
[19]Y. D. Lin, Y. Yamamoto, C. Y. Huang, C. L. Hsiung, F. Wu, K. Fujito, H. Ohta, J. S. Speck, S. P. DenBaars, and S. Nakamura, Appl. Phys. Express **3**, 082001 (2010).
[20]Y. Zhao, S. Tanaka, C. C. Pan, K. Fujito, D. Feezell, J. S. Speck, S. P. DenBaars, and S. Nakamura, Appl. Phys. Express **4**, 082104 (2011).
[21]C. Y. Huang, M. T. Hardy, K. Fujito, D. F. Feezell, J. S. Speck, S. P. Den-Baars, and S. Nakamura, Appl. Phys. Lett. **99**, 241115 (2011).
[22]D. S. Sizov, R. Bhat, A. Zakharian, K. Song, D. E. Allen, S. Coleman, and C. E. Zah, IEEE J. Sel. Top. Quantum Electron. **17**, 1390 (2011).
[23]C. Y. Huang, Q. Yan, Y. Zhao, K. Fujito, D. Feezell, C. G. V. de Walle, J. S. Speck, S. P. DenBaars, and S. Nakamura, Appl. Phys. Lett. **99**, 141114 (2011).
[24]J. Piprek, R. K. Sink, M. A. Hansen, J. E. Bowers, and S. P. DenBaars, Proc. SPIE **3944**, 28 (2000).
[25]K. A. Bulashevich, V. F. Mymrin, S. Yu. Karpov, I. A. Zhmakin, and A. I. Zhmakin, J. Comput. Phys. **213**, 214 (2006).
[26]C. K. Li and Y. R. Wu, IEEE Trans Electron Devices **59**, 400 (2012).
[27]F. Akyol, D. N. Nath, S. Krishnamoorthy, P. S. Park, and S. Rajan, Appl. Phys. Lett. **100**, 111118 (2012).